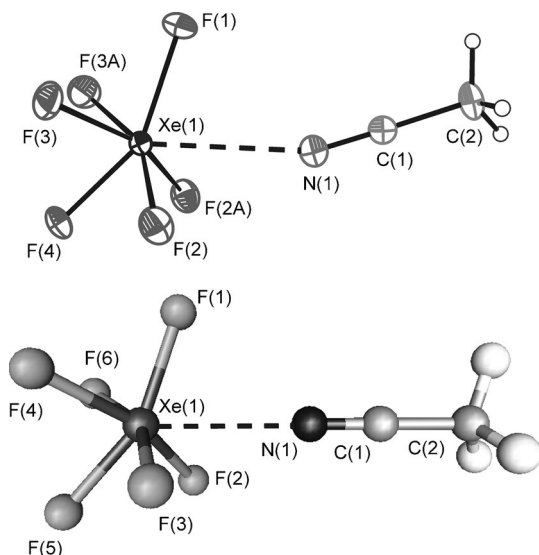




Little information on the solution structure of **1** could be garnered from its  $^{19}\text{F}$  and  $^{129}\text{Xe}$  NMR spectra in  $\text{SO}_2\text{ClF}$  (see the Supporting Information for a full discussion).

Single crystals of **1** and **2**· $\text{CH}_3\text{CN}$  suitable for X-ray crystal-structure determination were grown by slowly cooling their respective  $\text{SO}_2\text{ClF}$  and  $\text{CH}_3\text{CN}$ /Freon-114 solutions. The crystal structures of the isolated adducts and their calculated structures are in excellent agreement (Figure 1 and Figure 2, Tables S1 and S2; see the Supporting Information for a full discussion of the calculated geometries).



**Figure 1.** X-ray crystal structure of  $\text{F}_6\text{XeNCCH}_3$  (top). Ellipsoids are shown at the 50% probability level. The calculated geometry (PBE1PBE/avg-cc-pVTZ(-PP)) for  $\text{F}_6\text{XeNCCH}_3$  (bottom) is also shown.

The local symmetry of the  $\text{XeF}_6$  moiety in **1** is approximately  $C_{3v}$  (Figure S1), whereas its crystal site symmetry is  $C_s$ . The Xe–N distance (2.762(2) Å) is significantly longer than the  $\text{Xe}^{\text{II}}\text{--N}$  distances in  $[\text{C}_6\text{F}_5\text{XeNCCH}_3]^+$  (2.640(6)–2.610(11) Å),<sup>[22]</sup> but similar to the  $\text{Xe}^{\text{IV}}\text{--N}$  bond lengths in  $\text{F}_2\text{OXeNCCH}_3$  (2.808(5), 2.752(5) Å)<sup>[21]</sup> and  $[\text{C}_6\text{F}_5\text{XeF}_2]\cdot[\text{BF}_4]\cdot\text{NCCH}_3$  (2.742(4) Å).<sup>[20]</sup> The bond lengths are significantly shorter than the sum of the Xe and N van der Waals radii (3.71 Å),<sup>[23]</sup> but notably longer than  $\text{Xe}^{\text{II}}\text{--N}$  bonds (2.02(1)–2.236(4) Å).<sup>[19]</sup> The N1 atom of **1** is located on a pseudo- $C_3$  axis. The non-linear Xe1–N1–C1 angle (160.31(17)°) is likely the result of crystal packing and the deformability of this angle. The F atoms of the  $\text{XeF}_6$  moiety comprise two groups, where F1, F2, and F2A form the most open trigonal face proximate to N1 and opposite to the most closed face, F3, F3A, and F4. The Xe VELP presumably resides between the Xe–F1, Xe–F2, and Xe–F2A bonds of the more open face. Correspondingly, the F–Xe–F angles [F1–Xe1–F2 and F1–Xe1–F2A: 115.65(4)°; F2–Xe1–F2A: 105.92(6)°] proximate to N1 are considerably more open than those of the opposite triad [F3–Xe1–F4 and F3A–Xe1–F4: 79.93(4)°; F3–Xe1–F3A: 82.59(8)°]. The difference between the average F–Xe–F angles of the open and closed faces is 29.53(6)°. The Xe–F bonds of the open face are significantly longer [Xe1–F1: 1.9769(13) Å; Xe1–F2/F2A: 1.9451(8) Å] than

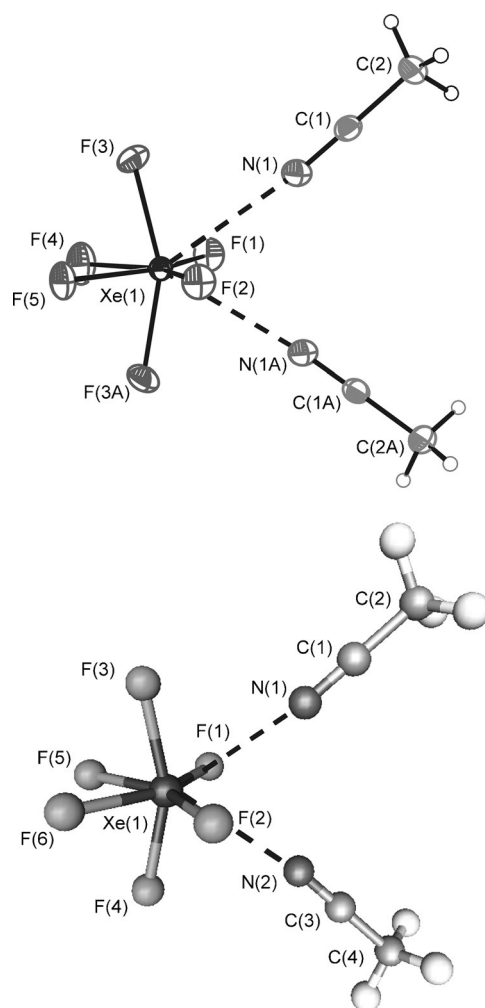


**Figure 2.** X-ray crystal structure of  $\text{F}_6\text{Xe}(\text{NCCH}_3)_2\cdot\text{CH}_3\text{CN}$ . The lattice  $\text{CH}_3\text{CN}$  molecule is not shown (top). Ellipsoids are shown at the 50% probability level. The calculated geometry (PBE1PBE/avg-cc-pVTZ(-PP)) for  $\text{F}_6\text{Xe}(\text{NCCH}_3)_2$  (bottom) is also shown.

those of the closed face [Xe–F3/F3A: 1.8560(9) Å; Xe–F4: 1.8601(12) Å]. At this time, it is not clear whether the  $C_{3v}$  geometry of **1** is imposed by  $\text{CH}_3\text{CN}$  or the presence of a sterically active Xe VELP. In the latter scenario, the Xe and N VELPs would oppose one another. Calculations are currently underway to ascertain the location of the Xe VELP. The average Xe–F bond length of **1** (1.907(2) Å) is comparable to those of other neutral  $\text{Xe}^{\text{VI}}$  species [ $\text{XeOF}_4$ : 1.890(2) Å;<sup>[24]</sup>  $\text{XeO}_2\text{F}_2$ : 1.899(3) Å<sup>[25]</sup>].

Compound **2**· $\text{CH}_3\text{CN}$  contains lattice  $\text{CH}_3\text{CN}$  molecules that lie in channels along the  $b$  axis and are twofold disordered along the  $a$  axis with a 50:50 population ratio (Figure S2). The crystal site symmetry of the  $\text{XeF}_6$  unit is  $C_s$ ; however, the isolated unit closely approximates  $C_{2v}$  symmetry. The Xe–N bond lengths (2.785(2) Å) of **2** are very similar to that of **1**. The N and C atoms of both coordinated  $\text{CH}_3\text{CN}$  molecules are approximately located on the pseudo-mirror plane bisecting the F1–Xe1–F2 and F4–Xe1–F5 angles. The Xe–F bonds of  $\text{F}_6\text{Xe}(\text{NCCH}_3)_2$  can be classified into three groups: two equatorial F atoms adjacent to the presumed

location of the Xe VELP [Xe1–F1: 1.981(2) Å; Xe1–F2: 1.9876(13) Å], two axial F atoms [Xe1–F3 and Xe1–F3A: 1.8936(11) Å], and two equatorial F atoms opposite to the Xe VELP [Xe1–F4: 1.868(2) Å; Xe1–F5: 1.873(2) Å]. The geometry of the XeF<sub>6</sub> moiety may be viewed as a C<sub>2v</sub>-distorted AX<sub>6</sub>E VSEPR arrangement (**5**) of the Xe VELP and six Xe–F bond pair domains, where the Xe VELP occupies a position between F1 and F2 in the equatorial Xe1–F1/F2–F4/F5 plane, causing the axial F3/F3A atoms to bend away from the equatorial VELP position towards F4/F5, resulting in an F3–Xe1–F3A angle of 156.90(7)°. When the Xe–N bonds (2.785(2) Å) are included in the description of the Xe coordination sphere, the F3/F3A, N1/N1A, and Xe1 atoms are seen to be coplanar within ±0.110 Å, with the Xe–N bonds avoiding the Xe VELP position.

The Raman spectra of **1** and **2**·CH<sub>3</sub>CN are shown in Figure 3. Selected experimental and calculated gas-phase (PBE1PBE/aug-cc-pVTZ(-PP)) frequencies and assignments

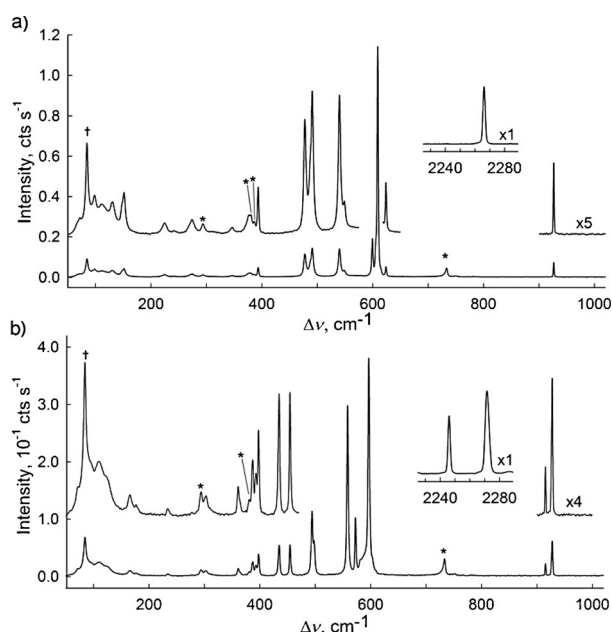


**Figure 3.** Raman spectra of a) **1** and b) **2**·CH<sub>3</sub>CN recorded at –150 °C using 1064 nm excitation. Symbols denote FEP sample tube lines (\*) and an instrumental artifact (†).

are listed in Table 1 and Table 2. Full lists, including the frequencies and assignments for coordinated CH<sub>3</sub>CN, are provided in Tables S3 and S4, along with a detailed discussion. The frequency trends are well reproduced by the calculations. Factor-group analyses were performed to account for splittings that occur on some bands (Tables S5 and S6).

In both adducts, high-frequency shifts occur for ν(CN), ν(CC), and δ(NCC), which is in accordance with the weak Xe–N bonding interaction that is indicated by the crystal structures and quantum-chemical calculations. The Xe–F stretches (**1**: 478–624 cm<sup>–1</sup>; **2**·CH<sub>3</sub>CN: 454–597 cm<sup>–1</sup>) occur in ranges similar to those reported for gas-phase and matrix-isolated XeF<sub>6</sub>,<sup>[6–8]</sup> but are shifted to lower frequencies. Weak bands at 129 and 110 cm<sup>–1</sup> in the Raman spectra of **1** and

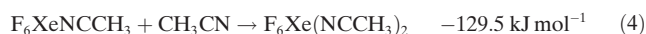
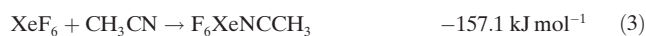
**Table 1:** Selected experimental and calculated Raman frequencies (cm<sup>–1</sup>) and assignments for F<sub>6</sub>XeNCCH<sub>3</sub>.<sup>[a]</sup>

Exp. <sup>[b]</sup>	Calculated <sup>[c]</sup>	Assignment
624.1(4) 609.1(100)	632.5(75)[184]	A <sub>1</sub> , ν <sub>s</sub> (XeF <sub>3b</sub> )
605.7 sh 599.5(13)	620.0(8)[211]	E, ν <sub>as</sub> (XeF <sub>3a</sub> ) + ν <sub>as</sub> (XeF <sub>3b</sub> )
548.4(1) 540.2(11)	557.5(18)[78]	A <sub>1</sub> , ν <sub>s</sub> (XeF <sub>3a</sub> )
491.0(12) 477.5(9)	504.5(14)[110]	E, ν <sub>as</sub> (XeF <sub>3a</sub> ) – ν <sub>as</sub> (XeF <sub>3b</sub> )
345.9(1)	335.3(1)[10] 334.2(1)[1]	A <sub>1</sub> , δ <sub>s</sub> (XeF <sub>3b</sub> ) E, δ <sub>as</sub> (XeF <sub>3a</sub> ) + δ <sub>as</sub> (XeF <sub>3b</sub> )
273.5(1)	246.8(1)[<1]	E, ρ <sub>r</sub> (XeF <sub>3a</sub> ) + ρ <sub>r</sub> (XeF <sub>3b</sub> )
223.9(1)	205.9(2)[17]	A <sub>1</sub> , δ <sub>s</sub> (XeF <sub>3a</sub> )
150.6(3) 147.2(<1)	149.2(<1)[1]	E, [δ <sub>as</sub> (XeF <sub>3a</sub> ) – δ <sub>as</sub> (XeF <sub>3b</sub> )] + δ(XeNC)
129.4(1)	106.1(1)[9]	A <sub>1</sub> , ν(XeN)

[a] See Table S3 for a full list of frequencies and assignments for all bands; abbreviations are given in the footnotes. [b] Values in parentheses denote relative Raman intensities. [c] PBE1PBE/aug-cc-pVTZ (-PP). Values in parentheses denote Raman intensities (Å<sup>2</sup> amu<sup>–1</sup>). Values in square brackets denote infrared intensities (km<sup>–1</sup>).

**2**·CH<sub>3</sub>CN, respectively, were assigned to ν(XeN). The low frequencies of the coupled δ(XeNC) modes (147–205 cm<sup>–1</sup>) are also consistent with weak Xe–N interactions and highly deformable Xe–N–C angles, and likely account for the non-linearity of this angle in the crystal structures of **1** and **2**·CH<sub>3</sub>CN.

Binding energies for the Xe–N interactions in **1** and **2** were determined at the MP2/aug-cc-pVTZ(-PP) level of theory [Eqs. (3)–(5)]. The energy for free XeF<sub>6</sub> was approximated from structure **3** (Table S7) and used because it was not possible to optimize **4** at the MP2 level of theory.<sup>[26]</sup> The energy differences between **3** and **4** are 0.79 (CCSD(T)/CBS)<sup>[12]</sup> and 7.53 kJ mol<sup>–1</sup> (CCSD(T)-F12b).<sup>[13]</sup>



In conclusion, the adducts **1** and **2**·CH<sub>3</sub>CN have been synthesized and structurally characterized by X-ray crystallography and Raman and NMR spectroscopy. They represent the first examples of Xe<sup>VI</sup>–N bonds, and their structures provide structural evidence that is consistent with the stereochemical activities of their Xe VELPs. Both adducts are well isolated from one another in their crystal lattices, based on the long intermolecular contacts observed among their structural units, and provide the only examples of

**Table 2:** Selected experimental and calculated Raman frequencies ( $\text{cm}^{-1}$ ) and assignments for  $\text{F}_6\text{Xe}(\text{NCCH}_3)_2$ .<sup>[a]</sup>

Exp. <sup>[b]</sup>	Calculated <sup>[c]</sup>	Assignment
596.6(100)	621.0(80)[161]	$A_{1g}, \nu_s(\text{XeF}_{2c}) + \nu_s(\text{XeF}_{2b})_{\text{small}}$
581.1(sh)	604.9(6)[229]	$B_{1g}, \nu_{as}(\text{XeF}_{2a}) + \nu_{as}(\text{XeF}_{2c})$
572.5(23)	598.7(6)[313]	$B_{2g}, \nu_{as}(\text{XeF}_{2b})$
558.5(78)	565.6(28)[24]	$A_{1g}, \nu_s(\text{XeF}_{2a}) + \nu_s(\text{XeF}_{2b}) - \nu_s(\text{XeF}_{2c})$
497.7(sh) 494.4(29)	509.1(16)[55]	$A_{1g}, \nu_s(\text{XeF}_{2a}) - \nu_s(\text{XeF}_{2b})$
454.3(13)	487.1(8)[136]	$B_{1g}, \nu_{as}(\text{XeF}_{2a}) - \nu_{as}(\text{XeF}_{2c})$
435.1(13)	407.2(1)[11]	$A_{1g}, \delta(\text{XeF}_{2c}) + (\text{XeF}_{2a})_{\text{small}}$
360.8(3)	335.9(<1)[3] 334.7(<1)[2]	$B_{2g}, \rho_r(\text{XeF}_{2b}) + \rho_w(\text{XeF}_{2c})$ $B_{1g}, \delta(\text{F}_a\text{XeF}_b) - \delta(\text{F}_a\text{XeF}_b)$
303.4(2)	278.9(1)[0]	$A_{2g}, \rho_t(\text{XeF}_{2b}) + \rho_t(\text{XeF}_{2c})$
293.3(<1)	260.3(<1)[17]	$A_{1g}, \delta(\text{XeF}_{2b}) - [\delta(\text{XeF}_{2a})]_{\text{small}}$
233.0(1)	201.6(<1)[10]	$A_{1g}, \delta(\text{XeF}_{2a}) + \delta(\text{XeF}_{2b}) -$ $[\rho(\text{XeF}_{2c}) + \delta(\text{XeNC})_{A+B}]_{\text{small}}$
176.2(<1) 165.1(2)	150.1(<1)[3] 149.5(<0.1)[0] 144.4(<0.1)[2]	$B_{2g}, \rho_r(\text{XeF}_{2b}) + (\delta(\text{XeNC})_{A+B})_{\text{ip}}$ $A_{2g}, \rho_t(\text{XeF}_{2a}) + \rho_t(\text{XeF}_{2c}) + (\delta(\text{XeNC})_{A+B})_{\text{oop}}$ $B_{1g}, \rho_r(\text{XeF}_{2a}) + \rho_r(\text{XeF}_{2c}) + (\delta(\text{XeNC})_{A+B})_{\text{oop}}$
109.6(1)	83.4(1)[<1] 76.6(<1)[6]	$B_{2g}, \rho_w(\text{XeF}_{2a}) + (\delta(\text{XeNC})_{A+B})_{\text{ip}}$ $A_{1g}, \nu(\text{XeN})_{A+B}$

[a] See Table S4 for a full list of frequencies and assignments for all bands; abbreviations are given in the footnotes. [b] Values in parentheses denote relative Raman intensities. [c] See the footnotes of Table 1.

a neutral ligand coordinated to  $\text{XeF}_6$ . The  $\text{CH}_3\text{CN}$  molecules weakly interact with Xe, thus the geometries of the  $\text{XeF}_6$  units in **1** and **2** provide excellent approximations of the gas-phase geometries of **4** and **5**. The  $\text{C}_{3v}$  geometry of ground-state  $\text{XeF}_6$  (**4**) has been accurately calculated for the gas-phase molecule.<sup>[12]</sup> Interestingly, the experimental geometrical parameters of the  $\text{XeF}_6$  moiety in **1** are in very good agreement with those of **4**. Computational investigations on the nature of the  $\text{Xe}^{\text{VI}}-\text{N}$  bonding in **1** and **2** and the localization of the Xe valence electron lone pair are currently in progress in our laboratory and will be reported in due course.

## Experimental Section

**Caution!** The adducts  $\text{F}_6\text{XeNCCH}_3$  and  $\text{F}_6\text{Xe}(\text{NCCH}_3)_2$  are highly energetic materials that may detonate when mechanically or thermally shocked (see the Supporting Information).

**Synthesis of 1:** Xenon hexafluoride (0.1796 g, 0.7322 mmol) was condensed under static vacuum at  $-196^\circ\text{C}$  into a FEP reaction tube (outer diameter: 0.25 inch) equipped with a Kel-F valve. Freon-114 (ca. 0.2 mL) was condensed onto the  $\text{XeF}_6$  at  $-196^\circ\text{C}$ . Direct contact between neat  $\text{CH}_3\text{CN}$  and  $\text{XeF}_6$  was avoided by condensing a stoichiometric amount of  $\text{CH}_3\text{CN}$  (0.0298 g, 0.7259 mmol) onto the reactor walls above the frozen Freon-114 and  $\text{XeF}_6$  layers at

$-196^\circ\text{C}$ . The sample was warmed to  $-78^\circ\text{C}$ , and frozen  $\text{CH}_3\text{CN}$  was carefully leached off the walls of the reactor with Freon-114. In this way,  $\text{CH}_3\text{CN}$  was diluted in Freon-114 prior to coming into contact with  $\text{XeF}_6$ . Moreover,  $\text{XeF}_6$  has a low solubility in Freon-114 at  $-78^\circ\text{C}$ . After most of the  $\text{CH}_3\text{CN}$  had dissolved, the sample was warmed to  $-40^\circ\text{C}$  and mixed for 10 min. Removal of Freon-114 by pumping at  $-78^\circ\text{C}$  resulted in a white powder corresponding to Freon-114 solvated  $\text{F}_6\text{XeNCCH}_3$ . Further pumping on the solvate at  $-78^\circ\text{C}$  resulted in removal of Freon-114, yielding a white powder corresponding to pure **1**.

**Synthesis of 2-CH<sub>3</sub>CN:** Using a procedure similar to that for **1**,  $\text{XeF}_6$  (0.1787 g, 0.7286 mmol) and  $\text{CH}_3\text{CN}$  (0.0896 g, 2.183 mmol) were combined. Removal of Freon-114 by pumping at  $-78^\circ\text{C}$  resulted in a white powder corresponding to pure **2-CH<sub>3</sub>CN**.

## Acknowledgements

We thank the Natural Sciences and Engineering Research Council of Canada for support in the form of a Discovery Grant (G.J.S.) and the Ontario Ministry of Training, Colleges, and Universities for graduate scholarships (J.H.).

**Keywords:** fluorine chemistry · noble-gas chemistry · Raman spectroscopy · xenon fluorides · X-ray crystallography

**How to cite:** *Angew. Chem. Int. Ed.* **2015**, *54*, 14169–14173  
*Angew. Chem.* **2015**, *127*, 14375–14379

- [1] L. S. Bartell, R. M. Gavin, Jr., H. B. Thompson, C. L. Chernick, *J. Chem. Phys.* **1965**, *43*, 2547–2548.
- [2] R. M. Gavin, Jr., L. S. Bartell, *J. Chem. Phys.* **1968**, *48*, 2460–2464.
- [3] L. S. Bartell, R. M. Gavin, Jr., *J. Chem. Phys.* **1968**, *48*, 2466–2483.
- [4] K. Hedberg, S. H. Peterson, R. R. Ryan, B. Weinstock, *J. Am. Chem. Soc.* **1967**, *89*, 6466–6469.
- [5] W. Harshberger, R. K. Bofn, S. H. Bauer, *J. Am. Chem. Soc.* **1967**, *89*, 6466–6469.
- [6] H. Kim, H. H. Claassen, E. Pearson, *Inorg. Chem.* **1968**, *7*, 616–617.
- [7] E. L. Gasner, H. H. Claassen, *Inorg. Chem.* **1967**, *6*, 1937–1938.
- [8] H. H. Claassen, G. L. Goodman, H. Kim, *J. Chem. Phys.* **1972**, *56*, 5042–5053.
- [9] J. N. Cutler, G. M. Bancroft, J. D. Bozek, K. H. Tan, G. J. Schrobilgen, *J. Am. Chem. Soc.* **1991**, *113*, 9125–9131.
- [10] J. S. Tse, D. J. Bristow, G. M. Bancroft, G. J. Schrobilgen, *Inorg. Chem.* **1983**, *22*, 2673–2677.
- [11] R. J. Gillespie, I. Hargittai, *The VSEPR Model of Molecular Geometry*, Allyn and Bacon, Boston, MA, **1991**.
- [12] K. A. Peterson, D. A. Dixon, H. Stoll, *J. Phys. Chem. A* **2012**, *116*, 9777–9782, and references therein.
- [13] L. Cheng, J. Gauss, J. F. Stanton, *J. Chem. Phys.* **2015**, *142*, 1–7.
- [14] S. Hoyer, T. Emmeler, K. Seppelt, *J. Fluorine Chem.* **2006**, *127*, 1415–1422.
- [15] A. Ellern, A. R. Mahjoub, K. Seppelt, *Angew. Chem. Int. Ed. Engl.* **1996**, *35*, 1123–1124; *Angew. Chem.* **1996**, *108*, 1198–1200.
- [16] G. J. Schrobilgen, J. H. Holloway, P. Granger, C. Brevard, *Inorg. Chem.* **1978**, *17*, 980–987.
- [17] K. Seppelt, N. Bartlett, *Z. Anorg. Allg. Chem.* **1977**, *436*, 122–126, and references therein.
- [18] M. Gerken, P. Hazendonk, J. Nieboer, G. J. Schrobilgen, *J. Fluorine Chem.* **2004**, *125*, 1163–1168.
- [19] G. L. Smith, G. J. Schrobilgen, *Inorg. Chem.* **2009**, *48*, 7714–7728, and references therein.

- [20] K. Koppe, J. Haner, H. P. A. Mercier, H.-J. Frohn, G. J. Schrobilgen, *Inorg. Chem.* **2014**, *53*, 11640–11661.
- [21] D. S. Brock, V. Bilir, H. P. A. Mercier, G. J. Schrobilgen, *J. Am. Chem. Soc.* **2007**, *129*, 3598–3611.
- [22] K. Koppe, H.-J. Frohn, H. P. A. Mercier, G. J. Schrobilgen, *Inorg. Chem.* **2008**, *47*, 3205–3217.
- [23] A. Bondi, *J. Phys. Chem.* **1964**, *68*, 441–451.
- [24] B. E. Pointner, R. J. Suontamo, G. J. Schrobilgen, *Inorg. Chem.* **2006**, *45*, 1517–1534.
- [25] G. J. Schrobilgen, N. LeBlond, D. A. Dixon, *Inorg. Chem.* **2000**, *39*, 2473–2487.
- [26] M. Kaupp, C. van Wüllen, R. Franke, F. Schmitz, W. Kutzelnigg, *J. Am. Chem. Soc.* **1996**, *118*, 11939–11950.

Received: August 14, 2015

Published online: September 21, 2015